


Article

Study on the Influence of the Performance Weakening of the Disconnectable Coupling (DC) Joint of Steel Support on the Retaining Structure of a Foundation Pit

Zhitian Xie ^{1,2}, Xiao Liu ¹ , Xiaokai Niu ^{2,*}, Jialong Jian ³, Chentao Xu ² and Jiahui Liao ²

¹ Faculty of Materials and Manufacturing, Beijing University of Technology, Beijing 100124, China; xiezt@bjut.edu.cn (Z.X.); liux@bjut.edu.cn (X.L.)

² Beijing Municipal Engineering Research Institute, Beijing 100037, China; wardy19930919@gmail.com (C.X.); LiaoJH0414@163.com (J.L.)

³ Key Laboratory of Urban Security and Disaster Engineering, Ministry of Education, Beijing University of Technology, Beijing 100124, China; jianjialong97@163.com

* Correspondence: metronxk@126.com

Abstract: In order to quantitatively study the influence of the weakening of the disconnectable coupling joint (DC joint) on the retaining structure, the pre-axial force retention performance of the steel support, the axial force of the steel support, the horizontal displacement of the diaphragm wall, and the ground settlement around the foundation pit were monitored during the construction of the foundation pit. The evolution process of the monitoring data was analyzed, and the corresponding numerical model verified by the monitoring data was established. The influence of the yield load of the DC joint, the initial compression stiffness, and the weakening of the pre-axial force on the stability of the retaining structure was studied by numerical simulation. The results show that the pre-axial force of steel support is only 67% of the design value when the soil below is not excavated within 24 h. The DC joint has a significant weakening effect on the steel support, which is unfavorable for the stability control of the foundation pit retaining structure. The pre-axial force and initial bending stiffness have a great influence on the stability of the retaining structure. When the yield load is not lower than that of the row piles, the DC joint has no effect on the stability of the retaining structure. This model can predict and analyze the deformation trend under different working conditions to a certain extent, providing certain reference value for safety plans during construction.

Keywords: foundation pit; steel support; disconnectable coupling joint; retaining structure; performance weakening



Citation: Xie, Z.; Liu, X.; Niu, X.; Jian, J.; Xu, C.; Liao, J. Study on the Influence of the Performance Weakening of the Disconnectable Coupling (DC) Joint of Steel Support on the Retaining Structure of a Foundation Pit. *Buildings* **2024**, *14*, 1330. <https://doi.org/10.3390/buildings14051330>

Academic Editor: Eugeniusz Koda

Received: 20 February 2024

Revised: 17 April 2024

Accepted: 20 April 2024

Published: 8 May 2024



Copyright: © 2024 by the authors. Licensee MDPI, Basel, Switzerland. This article is an open access article distributed under the terms and conditions of the Creative Commons Attribution (CC BY) license (<https://creativecommons.org/licenses/by/4.0/>).

1. Introduction

The disconnectable coupling joint (DC joint) serves as a critical component in the steel support system, designed to facilitate the adjustment of support lengths and maintain pre-axial forces [1–6], as illustrated in Figure 1. Comprising a movable segment, a fixed segment, and a steel wedge, the DC joint's structural configuration is depicted in Figure 2. The movable part consists of essential elements such as an end plate, a center rib plate, a jack bracket, a channel, and a stiffening rib. The end plate is attached to the steel beam, while the jack bracket provides a placement for the jack. The load is primarily carried by the center rib plate, the steel wedge, and the center plate of the fixed part. The fixed section includes steel pipes and flange plates in addition to the center plate, and the flange plate is fastened to the steel bracket and the DC joint. During the erection of the DC joint, a jack is gradually released to separate the movable part from the fixed part. Once the desired pre-axial force is achieved, a steel wedge is inserted between the movable and fixed parts. The jack is then retracted, completing the application of the pre-axial force. The DC joint plays a pivotal role in applying and maintaining pre-axial forces within the support system.

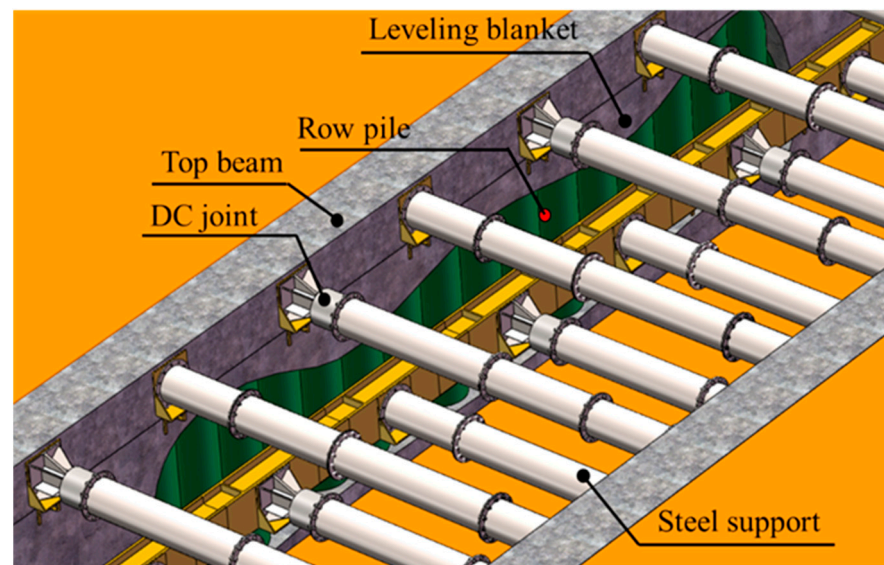


Figure 1. Steel bracing system.

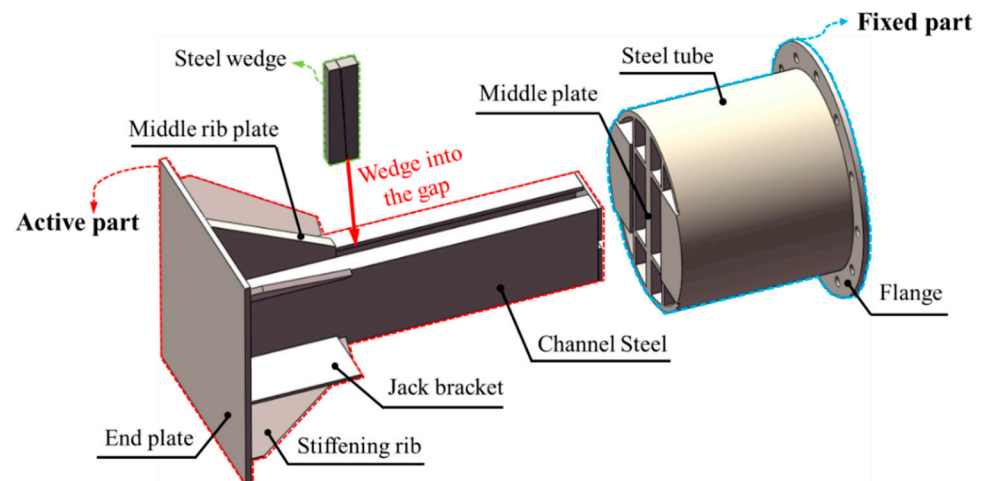


Figure 2. Structural form of disconnectable coupling with steel wedge.

However, studies have indicated that the bearing capacity and initial compression stiffness of DC joints are generally lower than those of the steel supports they connect, identifying them as a potential weak link within the support system [7–9]. This deficiency poses a significant risk to the structural integrity of the entire support system. The steel wedge is prone to loosening due to its structural design, leading to the dissipation of the pre-axial force [10]. As a result, the full potential of the steel supports is not realized [11], and the DC joint becomes a critical vulnerability in the steel support system, compromising the overall bearing capacity. The inadequate performance of these joints can lead to catastrophic failures, as evidenced by several foundation pit accidents [12–14].

One such accident occurred on 20 April 2004, when the Nicoll Highway foundation pit collapse in Singapore’s Metro loop was attributed to local buckling at the steel support–waist beam connection, diminishing the support’s bearing capacity and ultimately leading to the collapse of the entire pit [14,15]. Another incident involved the foundation pit collapse at Xianghu Station on Hangzhou Metro Line 1 on 15 November 2008. Zhang [16] highlighted the weakened link within the support system and the eccentric force at the DC joints as contributing factors to the accident. Zhou [17] underscored the delayed support as a crucial reason for the collapse, and Li [18] attributed the collapse to severe over-excavation and inadequate performance at the inner support connections. On 14 July 2010, a Beijing

Metro Line 15 foundation pit experienced a steel support detachment due to the loosening of the steel wedge at the DC joint, further underscoring the critical role of joints in the steel support system and their inadequate bearing capacity.

Despite these accidents, there remains a lack of quantitative analysis regarding the impact of DC joints' insufficient bearing capacity on the overall steel support system's performance. This study addresses this gap by monitoring the pre-axial force retention performance, the axial force of the steel supports, the horizontal displacement of the diaphragm wall, and the surface settlement around the pit at a station on Beijing Metro Line 17 during pit construction. The evolution of the monitoring data is analyzed, and a corresponding numerical model is developed, validated through comparison with the monitoring results. Utilizing this validated model, we investigate the influence of DC joints on the stability of the enclosure structure, examining the effects on the load carrying capacity, initial compression stiffness, and pre-axial force loss. The findings contribute to enhancing the understanding of the critical role of DC joints in the overall stability and performance of steel support systems.

2. Field Monitoring and Analysis of DC Joint Weakening Capacity

2.1. Engineering Situations

The main foundation pit of a station along Beijing Metro Line 17 adopts a steel support system with a DC joint. The north–south length of the pit is 363.5 m, and the width of the pit is 21.0~25.4 m. The east side of the pit is the construction site of the main pit of the station, and the west side is the traveling road and the building of the district in turn. The west side of the traveling road was a green belt and was then changed to a road. The main pit plan is shown in Figure 3.

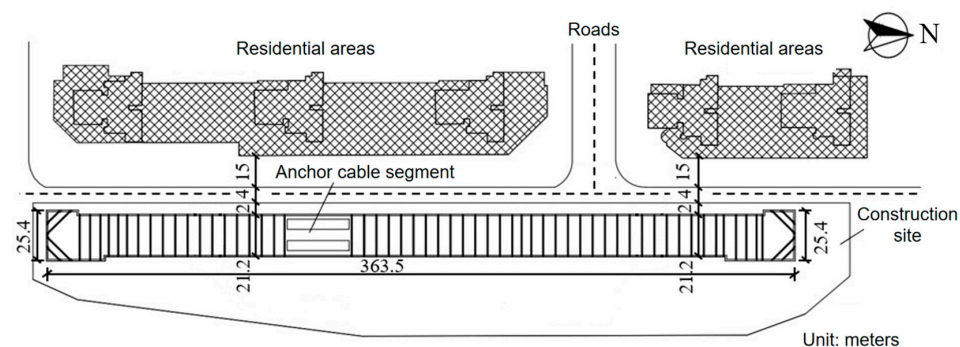


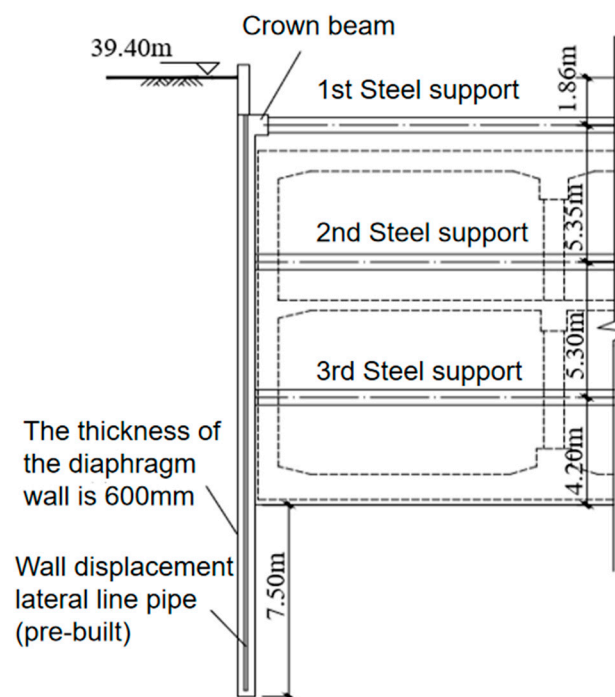
Figure 3. Planar graph of the foundation pit.

The geology of the pit location from top to bottom is as follows: ① miscellaneous fill, ② sandy silt, ③ silty clay, ④ sandy silt, ⑤ silty clay, ⑥ medium-fine sand, and ⑦ sand. The physical and mechanical indexes of the main layers of the site are shown in Table 1.

The width of the standard section of the pit enclosure structure is 21.0 m, and the excavation depth is about 17 m. A 600 mm thick diaphragm wall is used, and the embedment depth is 7.5 m. Three steel supports are used vertically, with the first steel pipe support spaced 6 m horizontally, and the second and the third steel pipe support spacing is 3 m horizontally. A section of the pit support structure is shown in Figure 4. The excavation of the foundation pit is carried out throughout descending construction.

Table 1. Physical and mechanical properties of each soil layer.

| Layer | Thickness/m | Unit Weight /kN·m ⁻³ | Cohesion/kPa | Internal Friction Angle/° | Elastic Modulus/MPa | Poisson Ratio |
|----------------------|-------------|------------------------------------|--------------|------------------------------|------------------------|---------------|
| ① miscellaneous fill | 2.0 | 16.00 | 8 | 10 | 3.00 | 0.3 |
| ② sandy silt | 5.5 | 20.20 | 18 | 26 | 6.00 | 0.3 |
| ③ silty clay | 5.5 | 19.40 | 24 | 29 | 7.50 | 0.3 |
| ④ sandy silt | 4.5 | 20.40 | 17 | 24 | 13.50 | 0.3 |
| ⑤ silty clay | 10.0 | 19.80 | 25 | 18 | 12.00 | 0.3 |
| ⑥ medium-fine sand | 12.0 | 20.8 | 0 | 32 | 30.00 | 0.3 |
| ⑦ sand | 20.0 | 20.8 | 0 | 35 | 40.00 | 0.3 |

**Figure 4.** Cross-sectional drawing of standard section of foundation pit.

The pre-axial force and design bearing capacity of each layer of support are shown in Table 2. The soil above the first steel support is named as the soil in the crown beam area, the soil between the first and second steel supports is called the first layer of soil, the soil between the second and third steel supports is called the second layer of soil, and the soil between the third steel support and the bottom of the pit is called the third layer of soil.

Table 2. Preloaded axial force and design bearing capacity of steel bracing.

| | 1st Steel Support | 2nd Steel Support | 3rd Steel Support |
|------------------------------|-------------------|-------------------|-------------------|
| Pre-Axial Force (kN) | 180 | 300 | 345 |
| Design Bearing Capacity (kN) | 1120 | 1950 | 2500 |

2.2. Monitoring Scheme

2.2.1. Measuring-Point Arrangement

The periphery of axis 12 on the south side of the pit was selected as the monitoring area, which contains three courses of eight steel supports and the settlement monitoring area around the pit. The monitoring content includes the axial force of the steel support, the horizontal displacement of the diaphragm wall, and surface settlement. The arrangement and numbering of measurement points are shown in Figure 5. ■ ZL represents the steel sup-

port axial force monitoring point, • CX represents the horizontal displacement monitoring of the ground-connected wall, and ▼ CJ represents the surface settlement monitoring point.

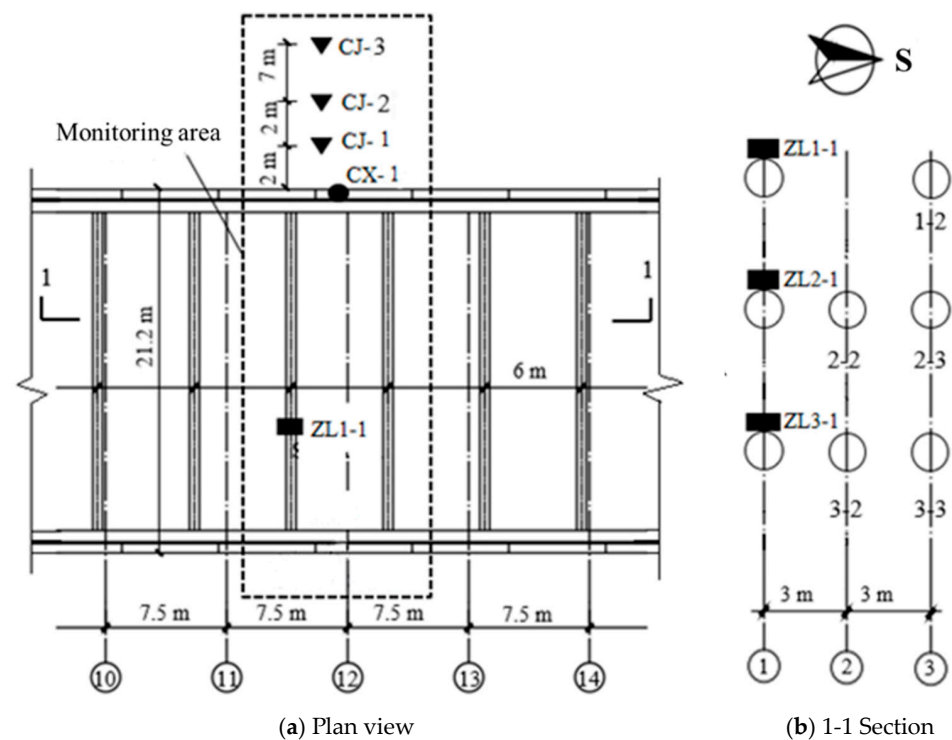


Figure 5. Monitoring arrangement (① etc. are the number of the axis).

2.2.2. Sampling Frequency

The monitoring frequency of the axial force of the steel support is 1 time per day, and the control index of the axial force of the steel support is the design bearing capacity of support in Table 2; the monitoring frequency of the horizontal displacement of the ground connecting wall and ground settlement is 1 time per day, and the control index of the horizontal displacement of the ground connecting wall and ground settlement is 30 mm. When the monitoring value is more than the control index, we have to stop the work for repair, and then we can start the work again after fixing it within the control standard. In the late construction period, the monitoring frequency is adjusted according to the site conditions. The construction date of each key process node is shown in Table 3.

Table 3. Time of key processes.

| Processes | Date |
|-------------------------------------|---------------|
| Erection of the First Steel Support | 20 March 2020 |
| Excavation of the First Layer | 8 April 2020 |
| Excavation of the Second Layer | 20 April 2020 |
| Excavation of the Third Layer | 29 April 2020 |
| Cushion Construction | 8 May 2020 |
| Bottom Floor Construction | 20 May 2020 |
| Removal of the Third Layer | 27 May 2020 |

2.3. Monitoring Results

2.3.1. Pre-Axial Force Retention Capacity

After the steel support is lifted and erected to the designated position, the pre-axial force is applied to the DC joints at different positions according to the design requirements. After the pre-axial force reaches the design value, the steel wedge is wedged in time, and the jack can be removed after the wedge is ready to complete the application of pre-axial

force. At the same time, the change in axial force during the installation process and 24 h after the completion of the installation was monitored, which was used to analyze the holding performance of the DC joint on the pre-axial force.

The time course patterns of steel support axial forces at the time of jack removal (0.5 h) and 1 h, 12 h, and 24 h after erection are given in Figure 6. The steel support axial force has a significant decrease at the moment of removing the jack, and the actual pre-axial force value of the steel support after the jack is removed is only 69~82% of the design value. One hour after erection, the pre-axial force of the three steel supports basically stabilized, about 75% of the design value. As the second and third steel supports were disturbed by the soil excavation below after erection, the monitoring value of axial force began to increase gradually, and the monitoring data at this time were the superposition of the pre-axial force value of the steel support and the axial force caused by the deformation of the foundation pit. The first steel support was not excavated for a long time after erection, so the value of the pre-axial force of the first steel support still gradually dissipated, and the monitoring value of the pre-axial force decreased to 67% of the design value of the pre-axial force after 24 h. Therefore, in the actual use of the steel support, the pre-axial force value cannot reach its design value, only about 70% of the design value of the pre-axial force value. The loss of pre-axial force is even more serious when the soil underneath is not excavated for a long period of time.

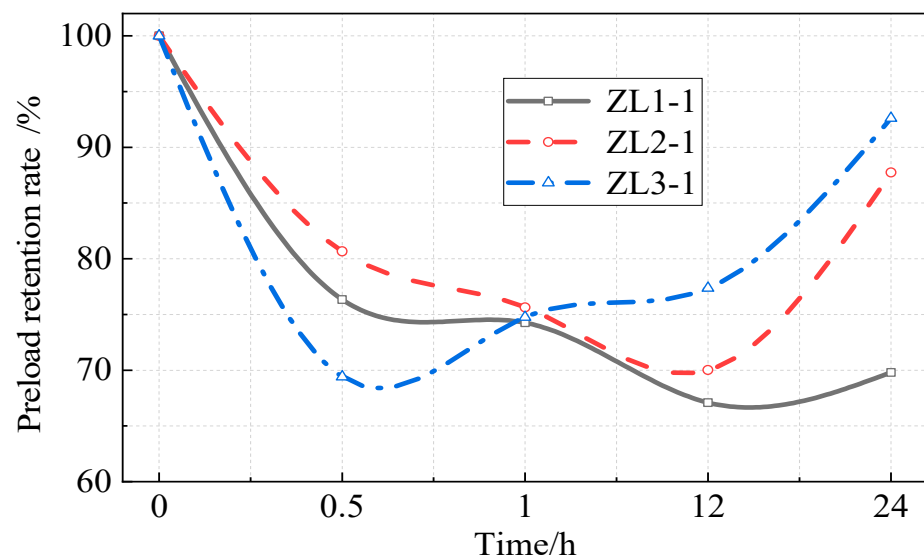


Figure 6. Preloading axial force retention condition.

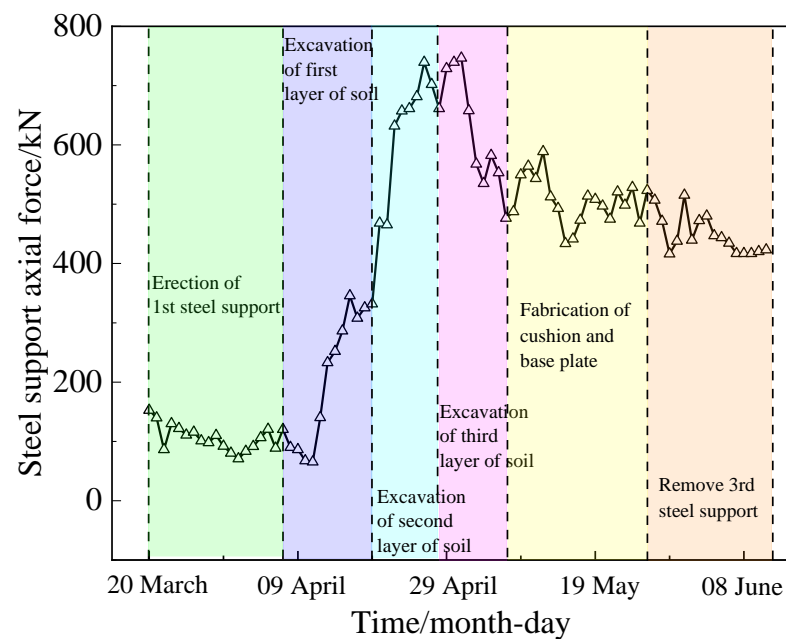
The loss of the steel support pre-axial force value is mainly due to the insufficient integrity of the DC joint structure and unreasonable force. When the steel wedge is wedged in, there will inevitably be gaps and asymmetric installation deviations, as shown in Figure 7, and after the jack is removed, a certain degree of misalignment between the steel wedge and the movable part and the fixed part occurs, resulting in the dissipation of the value of the pre-axial force. At the same time, due to the lack of structural integrity, the steel wedge is prone to misalignment when disturbed by the surrounding dynamic load, causing dissipation of the pre-axial force value.



Figure 7. Local contact of steel wedge.

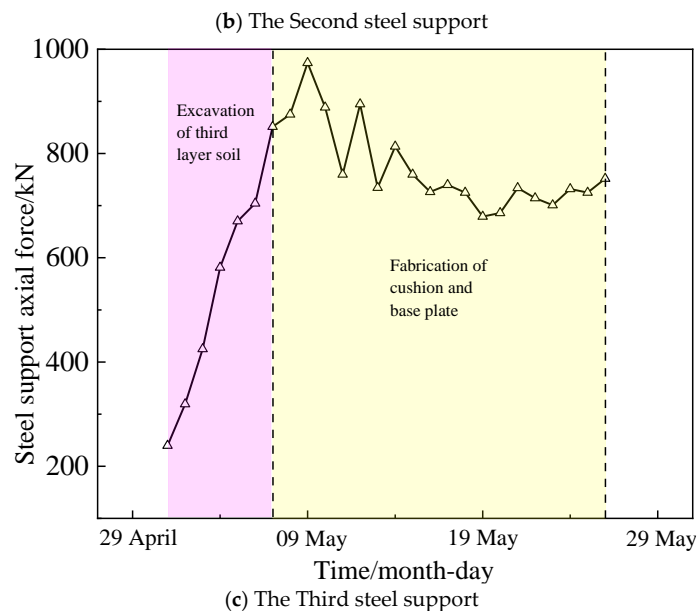
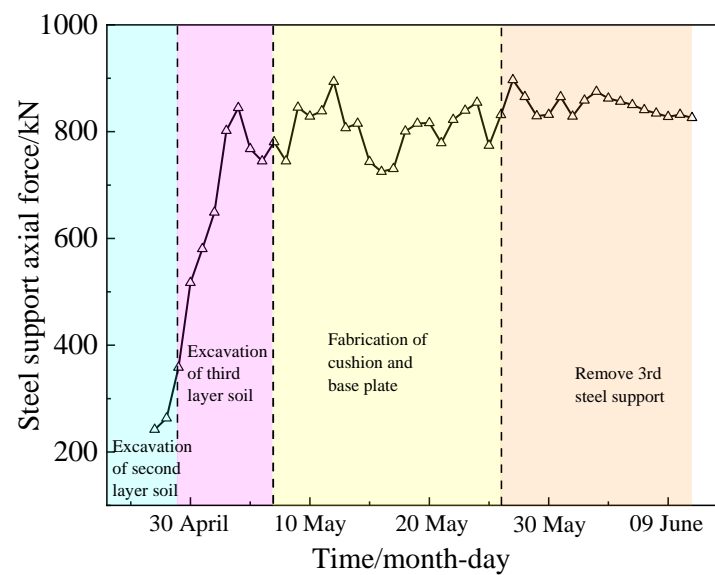
2.3.2. Bearing Capacity

Figure 8 lists steel supports 1-1, 2-1, and 3-1 in the construction process regarding the axial force evolution law; the maximum value of the three-steel-support axial force presents an overall trend of gradual increase from top to bottom. Each of the steel support force change laws are presented below; the excavation process of the soil body in the direction of steel support axial force increased rapidly. After the completion of the excavation of the soil body, the steel support axial force tends to stabilize in line with the general law of steel support axial force distribution.



(a) The First steel support

Figure 8. Cont.



(c) The Third steel support

Figure 8. Axial force evolution of steel bracing.

As can be seen from Figure 8a, between 20 March and 8 April, the axial force value at measurement point ZL1-1 gradually decreased. The axial force of the steel support gradually decreased because the soil underneath was not excavated immediately after the first support erection was completed, and the pre-axial force value of the steel support began to dissipate after it was disturbed by the surrounding soil. Afterwards, with the excavation of the first and second layers of soil, the axial force value of the ZL1-1 measurement point began to increase, and when the excavation of the second layer of soil was completed, the axial force of the DC joint reached a maximum value of 752 kN. During the excavation of the third layer of soil, the axial force value of the DC joint was gradually reduced to about 500 kN due to the disturbance of the first steel support by the construction, and the loss of axial force caused by the disturbance of the DC joint was mainly attributed to the fact that it is easy to be disturbed by construction, which causes the loss of axial force. During the subsequent construction process, the axial force value at measurement point ZL1-1 fluctuates within a small range, but tends to be stabilized on the whole.

As can be seen from Figure 8b, in the early stage of the excavation of the second layer of the soil body, the axial force value at the ZL2-1 measuring point was not collected due to the lack of monitoring conditions. In the late stage of the second soil excavation and the third soil excavation, the axial force value of ZL2-1 reached the maximum value of 844 kN, after which the axial force of the measuring point tended to be stable and fluctuated only in a small range.

Figure 8c gives the variation of the axial force at measurement point ZL3-1. After the excavation of the third layer of soil was completed, the axial force at measurement point ZL3-1 reached a maximum value of 973 kN. The subsequent axial force at measurement point ZL3-1 decreased slightly during the application of the bedding layer and the subgrade slab, but the overall tendency was stabilized at about 813 kN.

The monitoring data of measurement points ZL1-1, ZL2-1, and ZL3-1 all show a steady state after the removal of the third steel support, which is unreasonable. After the removal of the third steel support, the stress of the support system is redistributed, and the axial force of measurement points ZL1-1 and ZL2-1 should rise immediately and then stabilize after the bottom plate gradually exerts the load-bearing capacity, and this law has been verified in steel supports with BFW (bolt fasten wedge) active joints [19]. This indicates that the DC joint fails to respond in time to the stress redistribution in the footing and fails to exert its bearing capacity. This will inevitably cause excessive deformation of the row pile.

2.3.3. Horizontal Displacement of Diaphragm Wall

The data collected at measurement point CX-2 were more complete, so this measurement point was selected for analysis. The horizontal displacement of the diaphragm wall at measurement point CX-2 after the removal of the third steel support is shown in Figure 9. The maximum horizontal displacement of the wall occurred 12.1 m below the ground surface at the location of the original third support. The maximum horizontal displacement was 31.75 mm, which exceeded the deformation control value. This is dangerous for the deformation control of the pit.

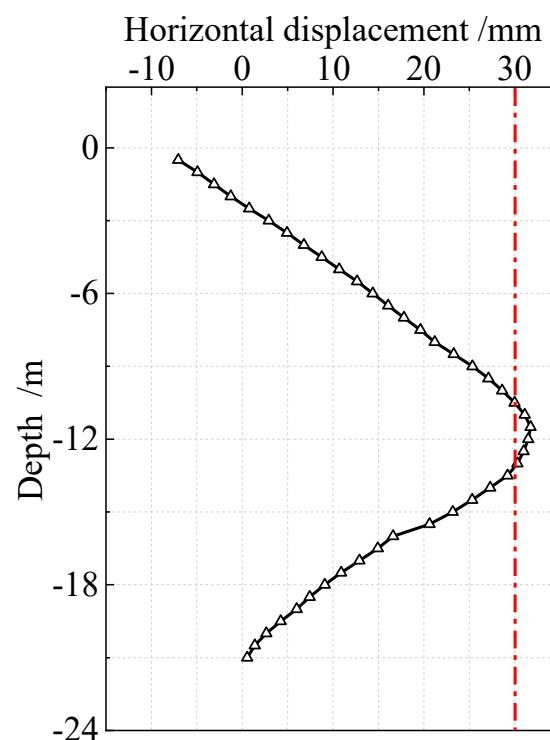


Figure 9. Cumulative displacement of diaphragm wall after foundation pit stabilization (red line is the threshold value of the horizontal displacement).

In order to analyze the change rule of the maximum horizontal displacement of the underground diaphragm wall, the maximum value of the accumulated horizontal displacement of the wall under different processes is calculated in Figure 10. In the period of time after the erection of the steel support, the soil below is not excavated, so in this period of time, the overall curve is smooth, and the maximum value of accumulated horizontal displacement of the wall is about 2 mm. Subsequent to the excavation of the first layer of soil, in the early stage of excavation, due to the excavation of shallow soil, the deformation of the wall has less influence, and the horizontal displacement of the wall is still small, which indicates that the enclosure structure is more stable in this period of time. In the late stage of the excavation of the first layer of soil, the wall deformation was affected more, and the maximum value of the accumulated horizontal displacement of the wall reached 9.56 mm after the completion of the excavation of the first layer of soil. In the excavation of the second and third layers of soil, the maximum value of the accumulated horizontal displacement still continued to increase, and after the completion of the excavation of the third layer of soil, the maximum value of the accumulated horizontal displacement of the wall reached 24.9 mm. In the construction of the mat foundation, the accumulated horizontal displacement of the wall began to converge to the same level. The cumulative horizontal displacement of the wall began to stabilize, and the maximum value of horizontal displacement was about 28.39 mm after the construction was completed. After the removal of the third steel support, the maximum value of the cumulative horizontal displacement of the wall had a certain magnitude of increase, which was related to the change rule of the bearing capacity in Section 2.3.2. As the third steel support is removed, the stress will be redistributed; at this time, the second and first steel support axial force should be increased rapidly to limit the horizontal displacement of the diaphragm wall through the role of steel support, but according to Section 2.3.2, it can be seen that after the removal of the third steel support, the axial force of the second and first steel support did not increase, which means that at this time, the steel support did not display its bearing capacity, so the horizontal displacement of the wall increased. After the removal of the third steel brace, the maximum accumulated horizontal displacement of the wall stabilized.

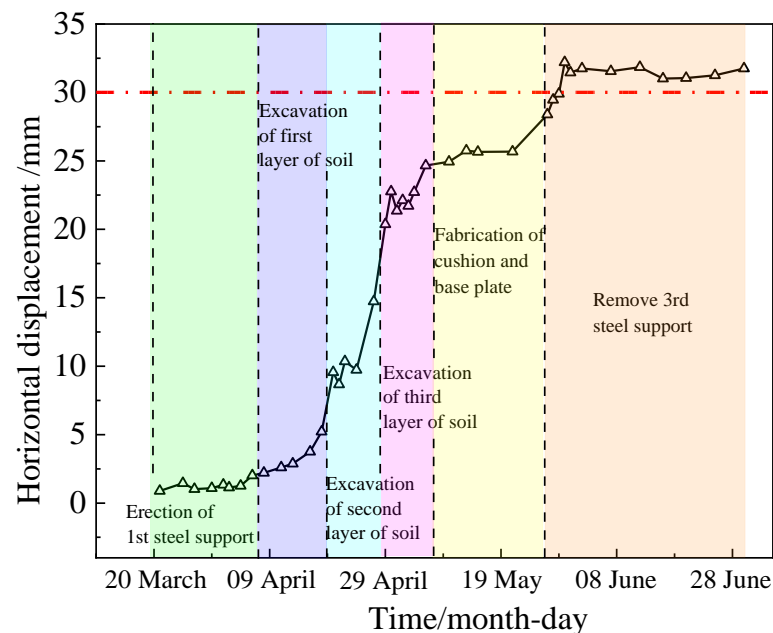
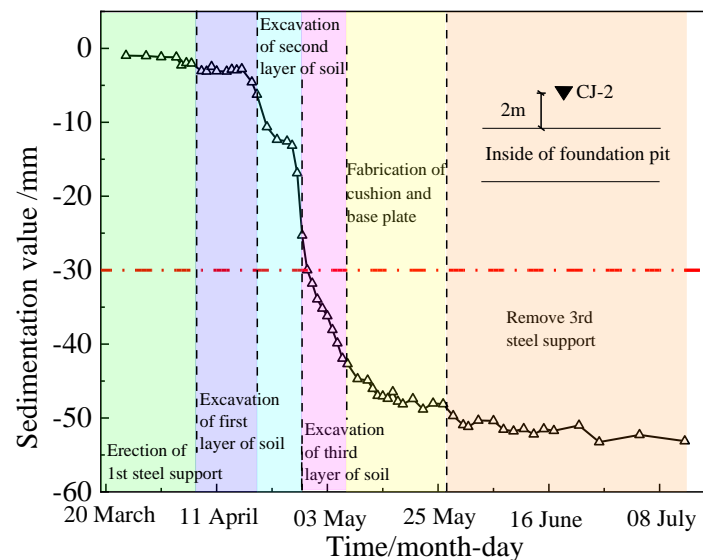


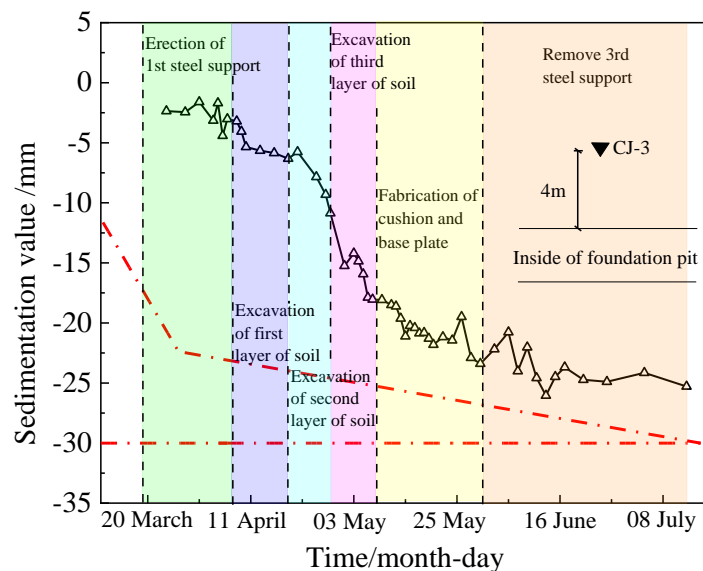
Figure 10. Evolution of the maximum cumulative horizontal displacement (red line is the threshold value of the horizontal displacement).

2.3.4. Surface Settlement around the Pit

Due to the influence of site monitoring conditions, the data of the settlement measurement point on the west side are more complete, so the measurement point on this side is analyzed. Figure 11 gives the settlement value of measuring points CJ-2, CJ-3, and CJ-4 and the change rule between construction processes. The settlement pattern of the three measuring points generally shows that the closer to the pit, the larger the settlement value. The final settlement values of measurement points CJ-2, CJ-3, and CJ-4 are 53.13 mm, 25.29 mm, and 6.13 mm, respectively.

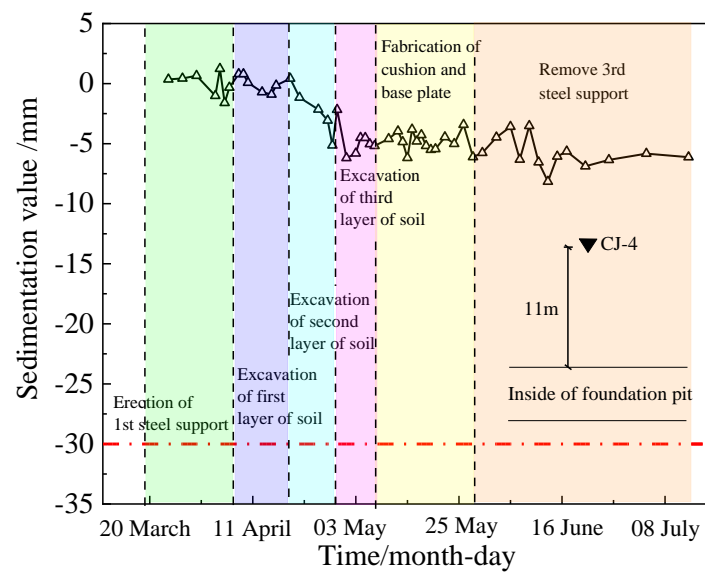


(a) Measuring Point CJ-2



(b) Measuring Point CJ-3

Figure 11. Cont.



(c) Measuring Point CJ-4

Figure 11. Evolution law of surface subsidence (red line is the threshold value of the sedimentation value).

From the change rule of measurement point CJ-2, shown in Figure 11a, it can be seen that the pit is more stable during the erection of steel supports and the excavation of the first layer of soil; the settlement value of measurement point CJ-2 is smaller, and the whole structure tends to be stable. The second layer of soil excavation has a greater impact on the periphery of the pit, and the settlement value of measurement point CJ-2 begins to increase rapidly; after the completion of the second layer of soil excavation, the settlement value of measurement point CJ-2 reaches 29.99 mm, which is close to the control standard of settlement. During the excavation of the third layer of the soil body, the settlement value of measuring point CJ-2 further increased and finally reached 44.71 mm, which exceeds the settlement control standard. In the subsequent process, the settlement value at measurement point CJ-2 still shows an increasing trend, but the overall change is small, and the settlement value tends to stabilize.

The variation rule of the settlement value of measurement point CJ-3 is closer to that of measurement point CJ-2, as shown in Figure 11b. During the period of steel support erection and the excavation of the first layer of soil, the pit is more stable; the settlement value of measurement point CJ-3 is smaller, and the settlement value of measurement point CJ-3 is only 5.76 mm at the end of the first layer of soil excavation. During the period of excavation of the second and third layers of soil, the settlement value of measurement point CJ-3 starts to increase rapidly. When the excavation of the third layer was completed, the settlement value of point CJ-3 was 18.08 mm. In the subsequent construction steps, the settlement value increased slightly, but the rate of increase was small, and the final settlement value was 25.29 mm, which was close to the settlement control index and exceeded the warning value of settlement control (80% of the settlement control index).

Measurement point CJ-4 was farther away from the specific pit, so the settlement values varied less throughout the construction period. The overall trend was a gradual increase in settlement. The stage with the greatest rate of increase in the settlement value is during the excavation of the second layer of soil. The variation rule of settlement at measurement point CJ-4 is shown in Figure 11c.

The settlement patterns around the pit observed at the three settlement measurement points are basically the same. In the initial process, the pit is less disturbed, and the settlement values are smaller. In the process of large-scale excavation, the settlement around the pit began to increase rapidly, and after the end of the excavation, the settlement

value of each measurement point tended to stabilize again. And the closer the pit is, the larger the settlement value is, and the more obvious the change rule is.

3. Numerical Analysis of the Effect of Weakened Bearing Capacity of DC Joints

3.1. Quantitative Analysis of Localized Weakening of Steel Supports

The on-site monitoring data showed that the steel support at the DC joint was not effective in controlling the deformation of the enclosure structure and controlling the settlement around the pit. The deformation of the enclosure structure and settlement around the pit exceeded the control standard, and the cumulative settlement value reached 52 mm, which was close to 1.8 times the control standard. Therefore, it is necessary to compare and analyze the bearing capacity of the DC joint and its matching equal-length steel support and establish a numerical model based on it to carry out a parametric study on the weakening of the bearing capacity of steel supports by DC joints.

Xie [20] gave load–displacement curves of steel supports with 609 mm OD and 12 mm, 14 mm, and 16 mm wall thicknesses equal to the length of the DC joint by numerical simulation. Zhang [21] obtained the mechanical properties of a DC joint by testing. The load–displacement curves of the three types of steel supports and the DC joint are listed in Figure 12. The bearing capacity of DC joints is much lower than any kind of steel support, and the yield load is only equivalent to 65.4% of 609-12, 54.7% of 609-14, and 45.9% of 609-16, and the initial compression stiffness is equivalent to 21.2% of 609-12, 19.9% of 609-14, and 18.7% of 609-16. This means that when a DC joint supporting a steel support with an outer diameter of 609 mm is used, it reduces the bearing capacity of the whole support member by about 54% and reduces the deformation control ability of the support member on the enclosure structure by 84%, which affects the stability of the enclosure structure of the foundation pit and increases the hidden danger of the foundation pit. It also causes a great waste of steel supports.

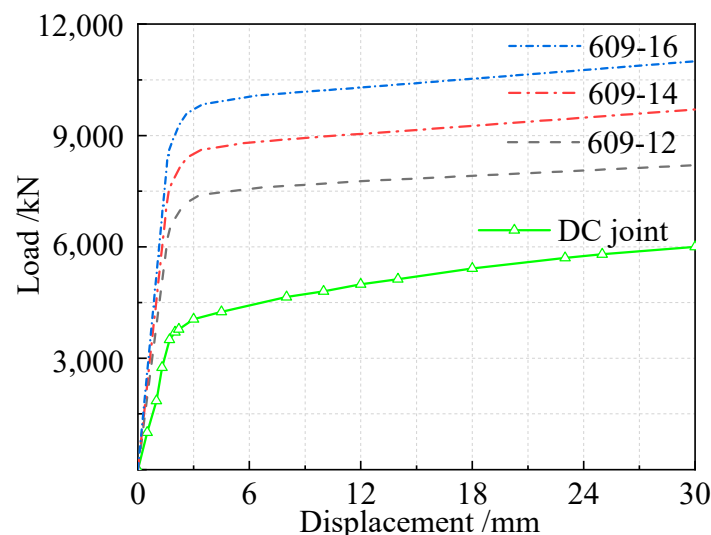


Figure 12. Comparison and analysis of bearing capacity of DC joint and steel support under axial load.

3.2. Numerical Study of a Foundation Pit Project of Beijing Metro Line 17

3.2.1. Modelling

1. Basic assumptions of the model

Because the actual project support structure, ground conditions, and construction situation are more complex, and the pit excavation is affected by spatial and temporal effects and other factors, the actual pit project is reasonably simplified and assumed to a certain extent to ensure that the calculation model can be optimized and the calculation efficiency can be improved without affecting the accuracy and authenticity of the calculation results. The specific assumptions and simplifications are as follows:

- The length of the deep foundation pit in this subway station is large and the width of the pit is not completely uniform. The area near the monitoring section in Figure 5 is selected and simplified as an equal-width pit for numerical analysis.
- The soil and structural materials are isotropic, with a Moore–Coulomb elastic–plastic principal model for the soil, an elastic model for the concrete, and an elastic–plastic model for the steel pipe and DC joint.
- Soils and diaphragm walls were simulated using 3D solid units, and DC joints and steel supports were simulated using 1D beam units.
- The pit was constructed through out-of-pit descent, and the groundwater level near the pit was found to be below the bottom of the pit in the actual observation, so the effect of groundwater was not considered in the finite element model.

2. Basic Dimensions of the Finite Element Model

The standard section of the foundation pit is about 21 m wide and 16.71 m deep, and the embedment depth of the diaphragm wall is 7.5 m. The steel supports are made of steel pipes with a 609 mm outer diameter and a 16 mm wall thickness. The spacing of the first steel support is 6 m, and the spacing of the second and third steel supports is 3 m. In order to reduce the influence of the model boundary effect on the numerical calculation of pit excavation, a 3–5-fold pit excavation depth is taken as the length of the model, and a 2–4-fold pit excavation depth is taken as the height of the model. Therefore, the length of the model is 120 m, the width is 42 m, and the height is 60 m. The X direction in the model corresponds to the east direction of the actual project, the Y direction in the model corresponds to the north direction of the actual project, and the Z direction in the model corresponds to the depth direction of the actual project; the finite element model is shown in Figure 13. The solid cells are meshed with C3D8, and all meshes are hexahedral meshes. The beam cells are meshed with B31. The soil mesh in the range of one times the width of the pit is encrypted, and a total of 54,777 meshes are divided.

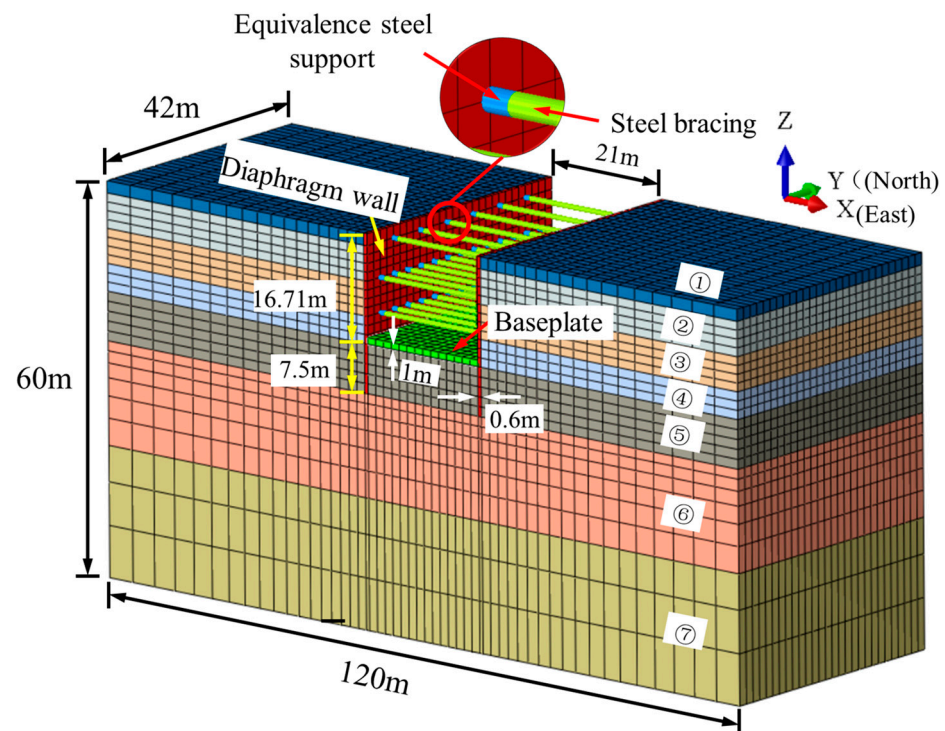


Figure 13. Finite element model of foundation pit (① etc. are the numbers of the layers shown in Table 1).

3. Material Parameters

Due to the large size of the pit, it is difficult to establish a refined DC joint model. In order to simplify the calculation, the original DC joint is equivalent to a 1 m long section of steel pipe support with a 609 mm OD and 16 mm wall thickness, and in order to restore the bearing capacity of the DC joint, it is necessary to discount the performance of the equivalent section of steel support. According to the study on the weakening rate of the steel support at the DC joint in Section 3.1, the yield load, initial compressive stiffness, and ultimate load at the DC joint are about 45.9% and 18.7% of the steel pipe support with an OD of 609 mm and a wall thickness of 16 mm. Therefore, the yield strength, elastic modulus, and ultimate strength of the equivalent section of the steel support are discounted according to this ratio, and the stress–strain relationship of the equivalent section of the steel support material after discounting is shown in Table 4 [22]. The stress–strain relationship of a normal steel support is selected according to Table 5 [20]. The underground diaphragm wall is made of C30 concrete and the bottom slab is made of C45 concrete. Other material parameters of the steel support, diaphragm wall, and base plate are shown in Table 6.

Table 4. Stress–strain relationship of equivalent steel bracing.

| | | | | | |
|----------------|---|--------|-----|-------|--------|
| Stresses (MPa) | 0 | 99.222 | 115 | 149.5 | 171.12 |
| Strains (%) | 0 | 0.1 | 0.3 | 10 | 17.7 |

Table 5. Stress–strain relation of Q235 steel.

| | | | | | | |
|----------------|---|-------|-----|-----|------|------|
| Stresses (MPa) | 0 | 215.7 | 250 | 325 | 372 | 402 |
| Strains (%) | 0 | 0.1 | 0.3 | 10 | 17.7 | 34.3 |

Table 6. Material parameters of bracing structure.

| Supporting Structure | Size Information (mm) | Materials | Unit Weight ($\text{kN}\cdot\text{m}^{-3}$) | Elastic Modulus (GPa) | Poisson Ratio |
|-------------------------------------|---|--------------|--|--------------------------|------------------|
| Steel Support | $\Phi = 609, t_D = 16, l_{D1} = 21,000$ | Q235 steel | 78.5 | 209 | 0.3 |
| Equivalent section steel support | $\Phi = 609, t_D = 16, l_{D2} = 1000$ | steel | 78.5 | 39.1 | 0.3 |
| Diaphragm Wall | $h_q = 600$ | C30 concrete | 25 | 30 | 0.2 |
| Bottom Floor | $h_b = 1000$ | C45 concrete | 25 | 45 | 0.2 |

Note: Φ is outer diameter of steel pipe, t_D is pipe wall thickness, l_{D1} is length of steel supports, l_{D2} is length of equivalent section steel supports, h_q is thickness of diaphragm wall, and h_b is thickness of bottom floor.

The material parameters of each soil layer in the finite element model are shown in Table 1.

4. Pre-axial Force Application

The effect of applying pre-axial force is achieved by changing the temperature of the steel support in the equivalent section to make it expand. The initial temperature of the finite element model is set to 0 °C. The following relationship exists between the steel support pre-axial force (F_a) and the temperature difference (ΔT):

$$\Delta T = \frac{F_a}{E_{\text{equ}} A_{\text{equ}} \alpha_1} \quad (1)$$

where E_{equ} is the elastic modulus of the steel support of the equivalent section, A_{equ} is the cross-sectional area of the steel support of the equivalent section, and α_1 is the coefficient of linear expansion of steel, which is taken as $1.25 \times 10^{-5}/^\circ\text{C}$.

According to Table 2, the design values of the pre-axial force of the first, second, and third steel supports are 180 kN, 300 kN, and 345 kN, respectively, while in the actual erection

process, the pre-axial force is greatly lost in a short time after the erection is completed. In order to make the numerical results more accurate, the pre-axial force of each steel support in the finite element model is adopted as the corresponding pre-axial force before the soil excavation below. Therefore, the preloaded axial forces of the second and third steel supports are 210 kN and 231.2 kN. The preloaded axial force of the first steel support is basically stable after 12 h of erection because the soil below has not been excavated for a long period of time after erection, and the preloaded axial force of the first steel support is adopted as the preloaded axial force 12 h after erection, which is 117 kN. The preloaded axial forces of the three steel supports are about 70% of the design value.

5. Contact Forms and Boundary Conditions

According to the collected data of the axial force of steel supports in the foundation pit, it can be seen that the steel support is always under pressure, which means that it is always in compression and always connected with the underground diaphragm wall, so the binding constraint is used between the steel support and the underground diaphragm wall. The soil body of the diaphragm wall is synergistically stressed by friction, and the contact form between the soil body and the diaphragm wall is set as surface-to-surface; the normal direction is set as hard contact and separation after contact is allowed; and the tangential direction is defined as penalized friction, isotropic, and the coefficient of friction is 0.577 [23]. Specific forms of contact between the individual components in the model are shown in Table 7.

Table 7. Contact settings for finite element models.

| Contact Part | Contact Type |
|---|--------------------|
| Soil–Diaphragm Wall | Surface-to-Surface |
| Diaphragm Wall–Steel Support | Tie |
| Soil–Bottom Floor | Tie |
| Steel Support–Equivalent section steel support | Tie |
| Diaphragm Wall–Equivalent section steel support | Tie |

The boundary conditions of the finite element model are set in the initial step of the ground stress equilibrium, and the displacement along the x direction is limited for the boundaries on the east and west sides of the soil body; the displacement along the y direction is limited for the boundaries on the south and north sides of the soil body and the underground diaphragm wall; and the displacement along the arbitrary direction is limited for the bottom of the soil body. The boundary conditions of the finite element model are shown in Figure 14.

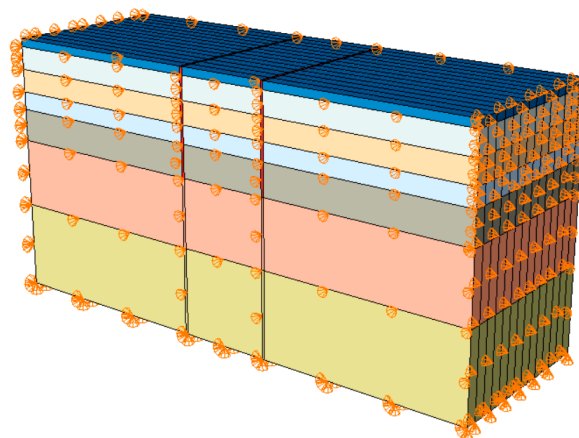
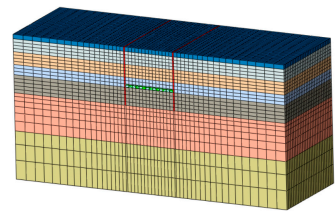
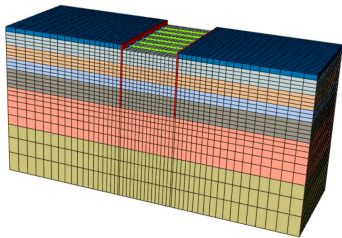
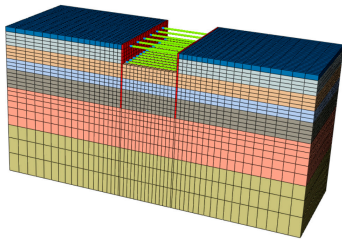
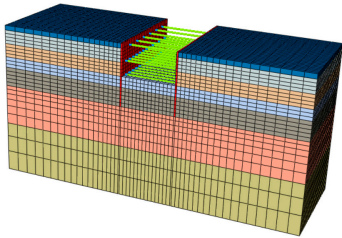
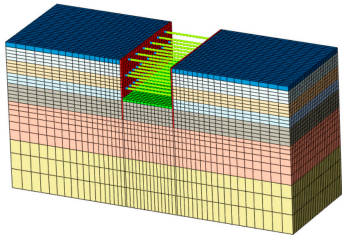
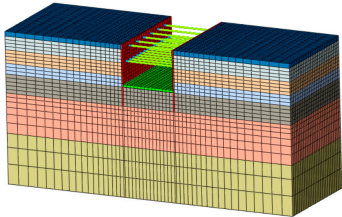


Figure 14. Boundary conditions of finite element model of foundation pit (the colors are the same as Figure 13).

6. Construction Process

In the actual project, the foundation pit excavation is a layered excavation, not a one-time excavation to the bottom of the foundation pit. In order to simulate the dynamic process of the foundation pit excavation in the actual project, six processes are set up according to the actual construction sequence, as shown in Table 8.

Table 8. Foundation pit excavation procedure.

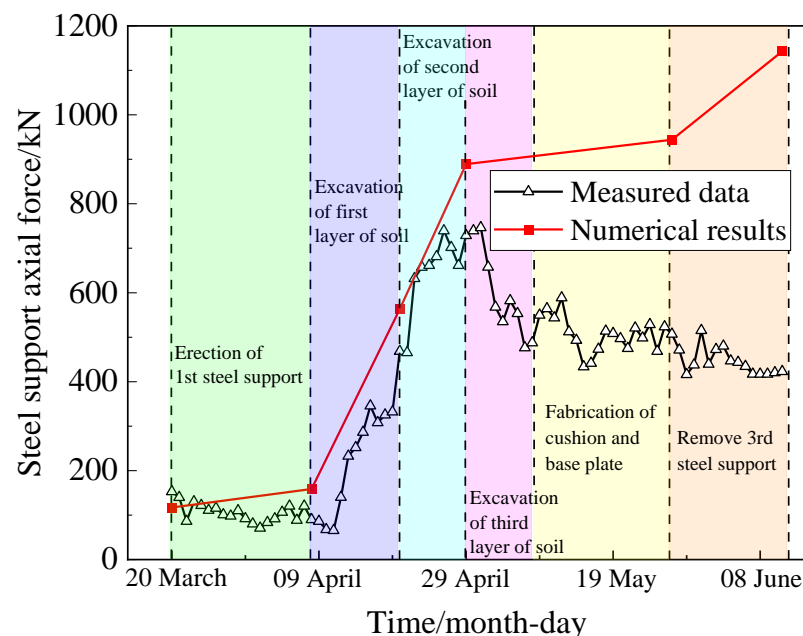
| Step | Construction Process | Construction Diagram |
|--------|--|---|
| Step 1 | Stress balance |  |
| Step 2 | Soil excavation in the crown beam area (1.86 m), erection of 1st steel support, application of pre-axial force |  |
| Step 3 | Excavation of 1st layer of soil (5.35 m), erection of 2nd steel support, application of pre-axial force |  |
| Step 4 | Excavation of 2nd layer of soil (5.3 m), erection of 3rd steel support, application of pre-axial force |  |
| Step 5 | Excavation of 3rd layer of soil (4.2 m), bottom floor construction |  |
| Step 6 | Removal of 3rd layer of steel support |  |

Since this research focuses on the influence of the steel support system on the stability of the enclosure structure without considering the influence of the diaphragm wall, the diaphragm wall will be set up in the process of geostatic stress balance in the soil body. Construction loads of 30 kPa and personnel loads were applied at the bottom of the pit after each step of soil excavation.

3.2.2. Analysis of Numerical Results

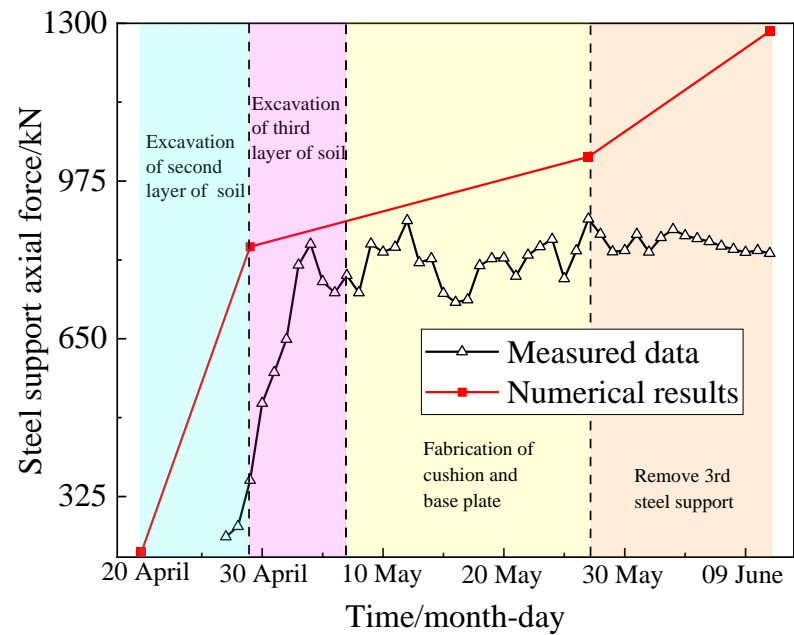
1. Comparative Analysis of the Numerical and Measured Results of the Axial Force of the Steel Support

The numerical results of the axial force of the first steel support and the measured results are shown in Figure 15a. The numerical results are larger than the measured results, but the general trends of the two coincide. Especially before the excavation of the third soil layer, the maximum error between the numerical results and the measured results is not more than 12%. In the excavation of the third layer of soil and the subsequent construction process, the numerical results showed an increasing trend, while the monitoring results showed a gradual decrease and finally remained stable, which is mainly due to the fact that in these steps, the construction site is in the stage of the largest workload, both soil excavation and structural operations, so the steel support is more disturbed, which is prone to causing the DC joint to loosen and reducing the axial force of the steel support. Zhang [16] applied a DC joint in this pit project and monitored the steel support axial force, and the change rule of the monitored steel support axial force was more consistent with the numerical simulation results in this section; especially after the removal of the third steel support, the axial force of the first steel support increased significantly. Therefore, it is further verified that the decrease in the first steel support axial force in the third soil excavation and the subsequent construction process is caused by the shortening of the steel support due to the loosening of the steel wedge.

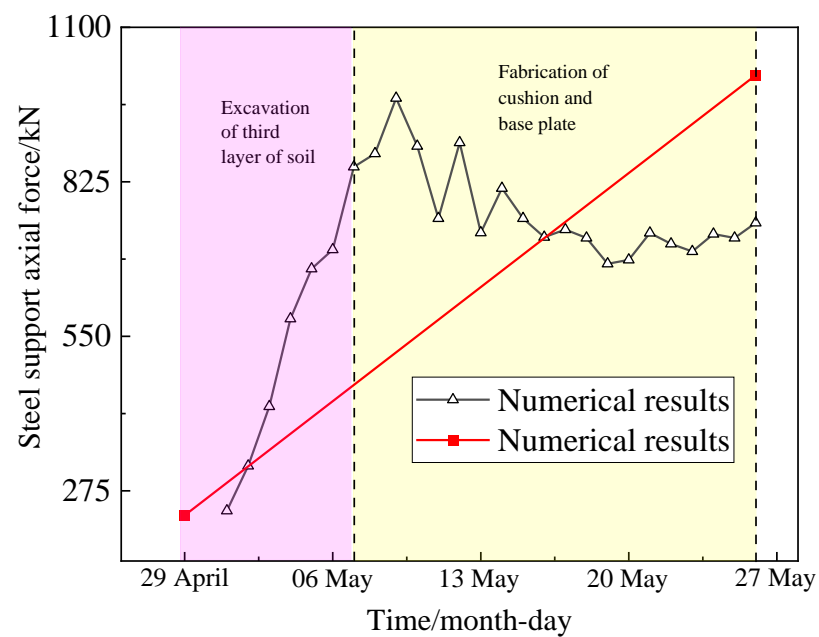


(a) The First Steel Support

Figure 15. Cont.



(b) The Second Steel Support



(c) The Third Steel Support

Figure 15. Axial force of steel bracing is compared with the measured results.

A comparative analysis of the numerical results and measured results for the second steel support under each construction process is given in Figure 15b. The numerical results are still larger than the measured results, but the overall trend matches. The axial force of the second steel support increased rapidly during the excavation of the second soil layer and the early stage of the excavation of the third soil layer. In the monitoring data, the maximum value of the second steel support axial force during the excavation of the third layer of soil and the application of bedding and subgrade is 893 kN, and in the numerical results, the maximum value of the second steel support axial force after the completion of

subgrade is 1024 kN; the error of the two is only 14%. Similar to the pattern in Figure 15a, the measured data after the removal of the third steel support were relatively smooth; the second steel support axial force did not increase rapidly, while the numerical results showed that the second steel support axial force increased by 223 kN in this process. The same numerical results showed that the pattern coincided with the pattern of change in the axial force of the DC joint steel support with BFW applied, which was monitored in [16].

The change rule of the third steel support axial force in measured data and numerical simulation is given in Figure 15c. Because the numerical simulation involves the excavation of the third layer of soil and the construction of the bedding and subgrade combined into one calculation step, there are only two data points, which can not fully reflect the change rule in this section of the process. However, during the process of the excavation of the third layer of soil and the construction of the bedding and subgrade, the maximum measured axial force of the third steel support is 973 kN and the numerical result is 1014 kN, which are in good agreement with each other.

2. Comparative Analysis of Numerical and Measured Horizontal Displacements of Diaphragm Walls

Figure 16 shows the comparison analysis of the numerical results of the horizontal displacement of the wall body under each process with the measured results, as well as showing the measured data for the removal of the third steel support after the horizontal displacement of the wall, and the numerical results of process 6 for the same construction step. It can be seen that the change rule of the two curves is almost the same, and the maximum displacement of the wall after the removal of the third steel support appeared at the original location of the third steel support. The numerical results are slightly smaller than the measured data, and the difference is about 2.4 mm. From process 2 to process 5, the maximum horizontal displacement of the wall body increases gradually, and the location of the maximum horizontal displacement of the wall body moves downward gradually with the excavation of the foundation pit.

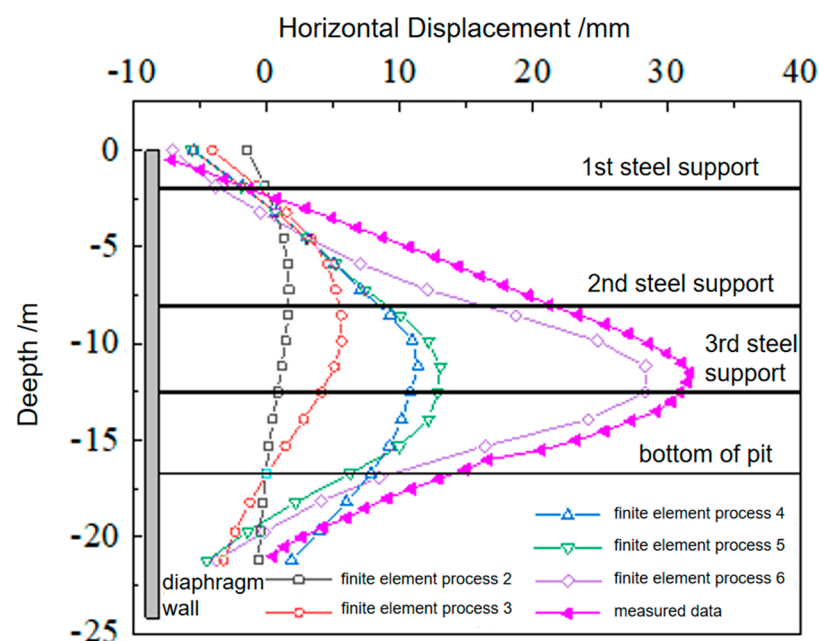


Figure 16. Horizontal displacement is compared with the measured results.

Figure 17 gives the change rule of the maximum horizontal displacement of the diaphragm wall's numerical results and measured results under each process. The overall rule of change is more consistent, especially in the second layer of soil body excavation before the numerical results and measured results match better. After the excavation of

the second layer of soil and in the early stage of the excavation of the third layer of soil, the measured data have a larger increase than the numerical results in the construction process, which is mainly due to the fact that, for numerical analysis, the third layer of soil excavation and the construction of bedding sub-slabs are combined into a single step, and the sub-slabs limit the horizontal deformation of the diaphragm walls. During the removal of the third steel support, the numerical results increased more than the measured data; this is due to the fact that the removal of the steel support in the actual project is gradual, the data have a significant increase when the steel support is removed around the measurement point, and the removal of the subsequent support is accompanied by the construction of other structures, so the data at the point of measurement begin to level off and the increase is small. In the finite element analysis, the steel support removal was an overall removal; therefore, the removal of the third steel support in the numerical results caused a sharp increase in the maximum horizontal displacement of the wall.

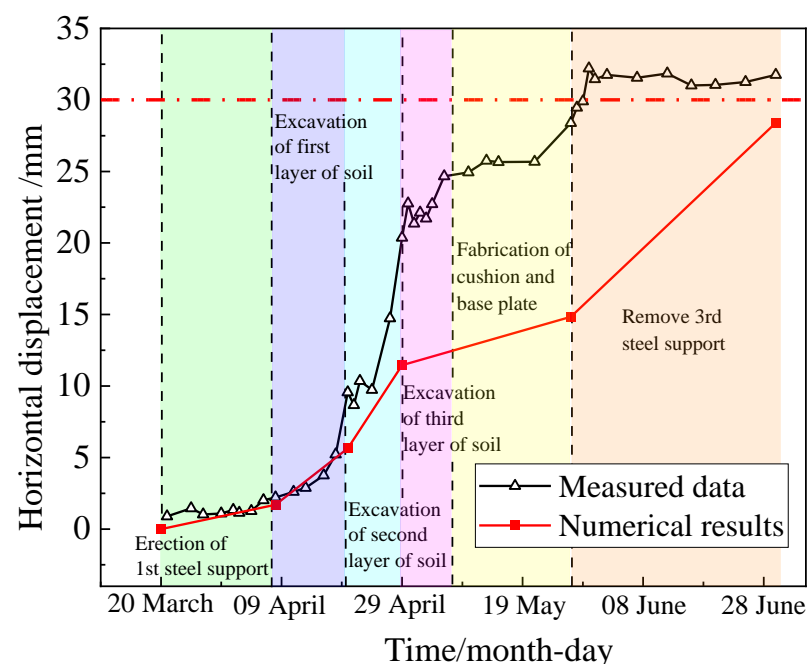
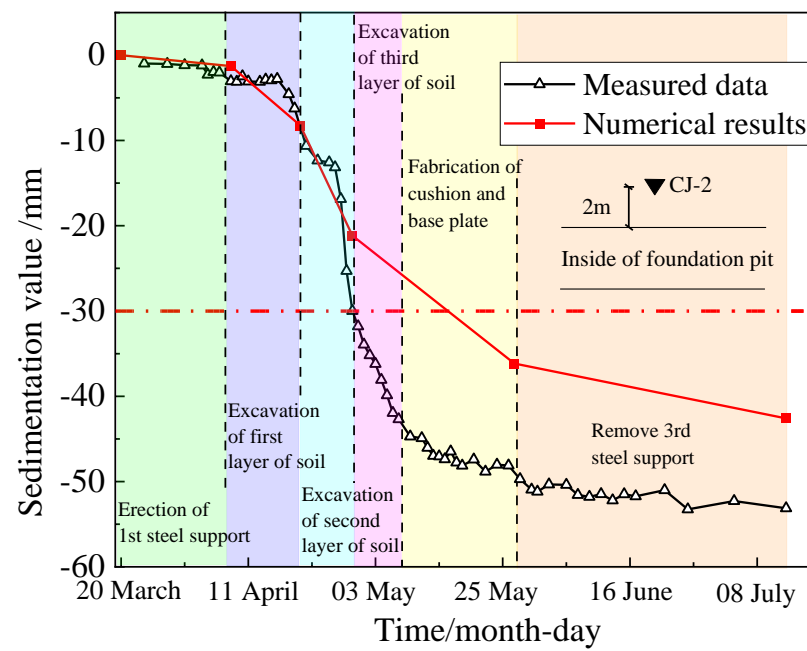


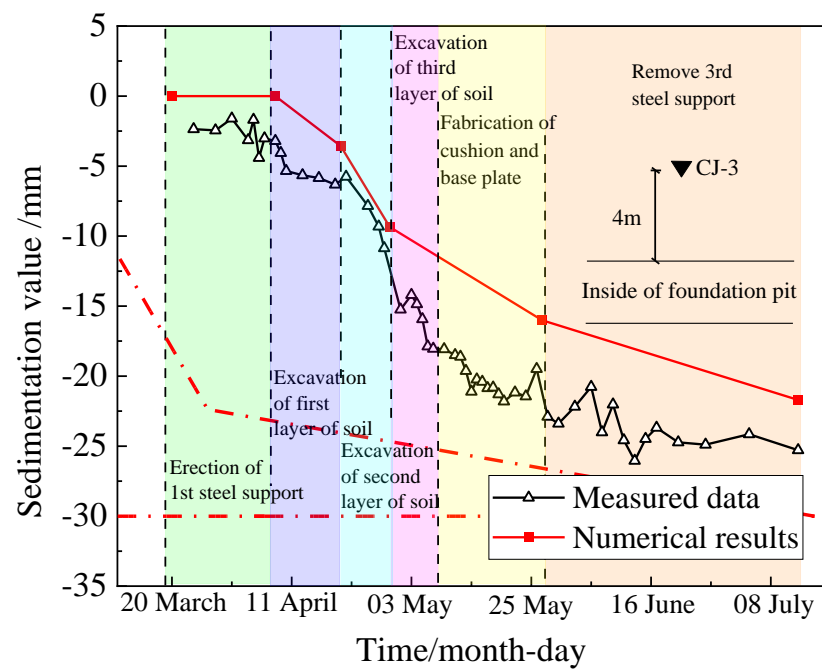
Figure 17. Maximum horizontal displacement of the envelope is compared with the measured results.

3. Comparative Analysis of Numerical and Measured Results of Surface Settlement

Figure 18 shows the numerical results of the settlement curve around the pit and the comparative analysis of the measured data; the change rule of the settlement curve at the three measurement points is in good agreement, and the farther away from the pit, the closer the monitoring data are to the numerical results. The main reason is that the closer the measurement point is to the pit, the greater the influence of pit excavation and enclosure structure construction, and the actual construction environment is much more complex than the numerical simulation. The numerical results of the settlement curves at the three measurement points and the measured data are basically in line with the rule of change of the numerical analysis results and are more satisfactory; the settlement is smaller. In the excavation of the third layer of soil and the application of bedding slabs, also due to the numerical simulation of these two steps being combined into one construction step, under the limitations of the subgrade, the numerical analysis of the surface settlement change is smaller. In the process of removing the third steel support, both the numerical results and the measured data showed a slight increase in settlement values, but the increase was smaller.

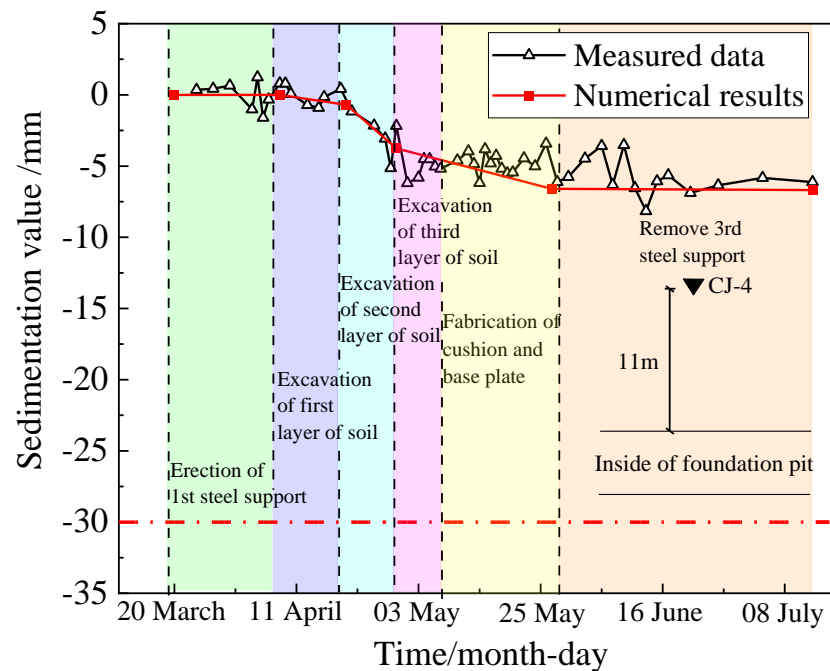


(a) Measuring Point CJ-2



(b) Measuring Point CJ-3

Figure 18. Cont.



(c) Measuring Point CJ-4

Figure 18. Comparison and analysis of numerical results and measured data of surface subsidence.

According to the comparative analysis of the numerical results and measured data of the steel support axial force, the horizontal displacement of the diaphragm wall, and the surface settlement around the foundation pit, the numerical results are in complete agreement with the trend of the measured data. It is verified that the simulation method in this section for the DC joint equivalent to steel support is feasible. And before the excavation of the third layer of soil, the numerical results are in good agreement with the measured data, and the errors are all within 20%. In the subsequent construction process, due to the disturbance of the complex construction environment at the construction site, the steel wedge at the DC joint was loosened, and the axial force of the steel support was not well maintained, so the axial force of the steel support in the measured data did not increase, while the deformation of the enclosure structure increased more, resulting in a slight difference between the numerical results and the measured data. However, the results of the comparative analysis show that the numerical model established in this paper with the corresponding pit project of Beijing Metro Line 17 is basically able to reflect the force and deformation law of the pit, and the material parameters, contact form, and boundary conditions set in the model are reasonable, which can be used to analyze the influence of the local weakening of steel support on the stability of the enclosure structure under different conditions.

3.3. Influence of the Degree of DC Joint Weakening on the Stability of Pit Enclosure Structures

The measured data from the construction site showed that the maximum horizontal displacement of the enclosure exceeded the control criteria due to the weakening effect of the DC joints on the steel supports. The weakening of the DC joint on the steel support is mainly manifested in the weakening of the pre-axial force retention performance, compressive stiffness, and yield load. Therefore, using the numerical model established in Section 3.2, the effects of different steel supports' initial pre-axial force, compressive stiffness, and yield load on the stability of the enclosure structure were analyzed, and the different types of weakening and the degree of weakening are listed in Table 9. The elastic modulus and yield load reflect the effects of the initial compressive stiffness and yield load at the DC joint, respectively, because the cross-sectional area of the equivalent steel support

is certain. The numerical model numbers are in the form of “JK”, where JK2 is the model developed in Section 3.2 of this paper.

Table 9. Finite element models of different weakening types.

| Number | Actual Value of Pre-Axial Force /Design Value of Pre-Axial Force | Elastic Modulus (GPa) | Yield Strength (MPa) |
|--------|---|-----------------------|----------------------|
| JK1 | 0% | 45.94 | 108.1 |
| JK2 | 70% | 45.94 | 108.1 |
| JK3 | 100% | 45.94 | 108.1 |
| JK4 | 70% | 45.94 | 235 |
| JK5 | 70% | 206 | 108.1 |

3.3.1. Influence of Pre-Axial Force

As shown in Figure 19, the pre-axial force applied to the steel support during erection is favorable for the deformation control of the enclosure structure. The effect of pre-axial force on the horizontal displacement of the enclosure structure is small when the first and second layers of soil are excavated, and the effect of pre-axial force on the horizontal displacement of the enclosure structure becomes more obvious when the third layer of soil is excavated. When no pre-axial force is applied, the maximum horizontal displacement of the enclosure structure after the removal of the third steel support exceeds the control standard and reaches 31.7 mm, whereas when the pre-axial force is applied at 70% of the design value, the maximum horizontal displacement of the enclosure structure can be controlled within the standard range. When the pre-axial force is fully applied according to the design requirements, the maximum horizontal displacement of the enclosure structure after the removal of the third steel support is 27 mm. According to Figure 20, it can be seen that the horizontal displacement of the enclosure structure is larger when the pre-axial force is not applied. And the pre-axial force applied to 70% or 100% does not seem to have much effect on the deformation of the enclosure structure. According to the observation and data analysis at the construction site, it is found that the law reflected in the actual project is slightly different from the numerical analysis results, and the serious loss of pre-axial force at the DC joint during erection is mainly due to the problems of loosening of the steel wedge and point contact at the steel wedge caused by the unreasonable structure. In the subsequent construction, the loosening of the steel wedge at the DC joint and the point contact problem at the steel wedge will make the axial force holding performance of the steel support decrease; the deformation of the enclosure structure will increase rapidly, and the steel support cannot make the stress redistribution of the enclosure structure accordingly in time. These cannot be realized by finite element analysis, so the numerical results show that the pre-axial force applied to 70% and 100% of the design value has little effect on the maximum horizontal displacement of the enclosure structure. In the actual project, the effect of pre-axial force applied to 70% or 100% of the design value on the maximum horizontal displacement of the enclosure will be greater than the numerical results.

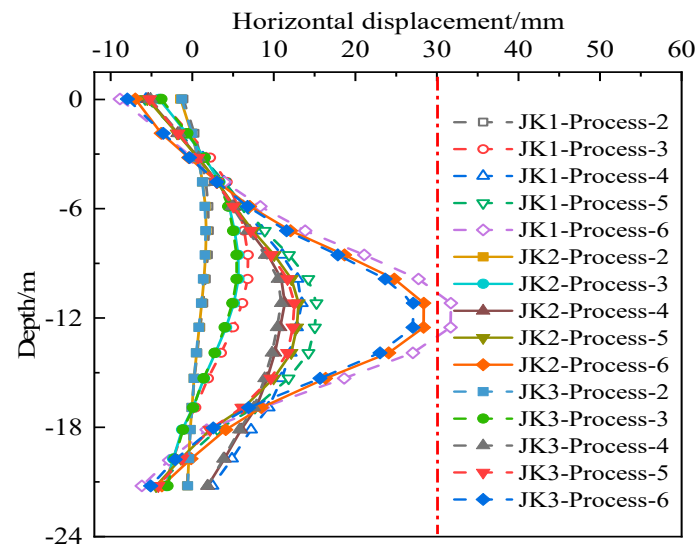


Figure 19. Influence of pre-axial force on horizontal displacement of envelope structure.

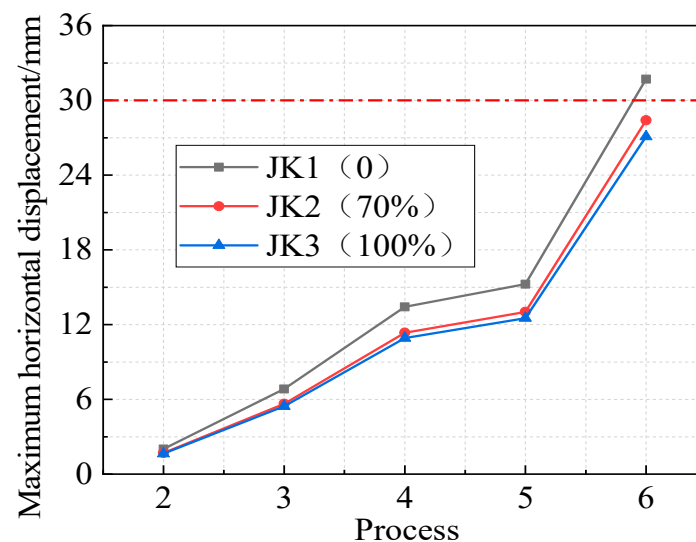


Figure 20. Variation law of maximum horizontal displacement of envelope under different pre-axial forces.

3.3.2. Influence of Bearing Capacity

Figure 21 gives the effect of the weakening of the steel support bearing capacity on the deformation pattern of the enclosure structure, and the weakening of the yield load at the DC joint at 46% of the standard section of the steel support has no effect on the deformation of the enclosure structure. This is mainly due to the fact that the actual load on the steel support is much smaller than the yield load of the steel support. As shown in the von Mises stress cloud in Figure 22, after the removal of the third steel support, the stress of the second steel support reaches the maximum, and it is only 39.4 MPa, which is much smaller than the yield stress of the steel support of 235 MPa and the stress after weakening of the DC joint of 108.1 MPa. Although the numerical analysis cannot take into account the installation error during the construction process, the unevenness of the diaphragm wall caused by the eccentric load, etc., it can also be seen that the current design of the bearing capacity of steel support is too conservative. At the same time, it is unreasonable to increase the outer diameter and wall thickness of the steel support to improve the bearing capacity of the steel support, and attention should be paid to the influence of DC joints on the lack of axial force retention performance. Figure 23 shows the change rule of the

maximum horizontal displacement of the enclosure structure at different levels of bearing capacity, and the two curves are completely overlapped.

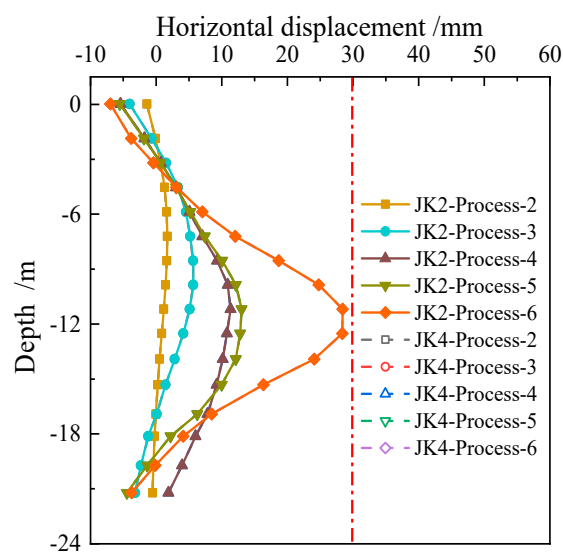


Figure 21. Influence of bearing capacity on horizontal displacement of envelope structure.

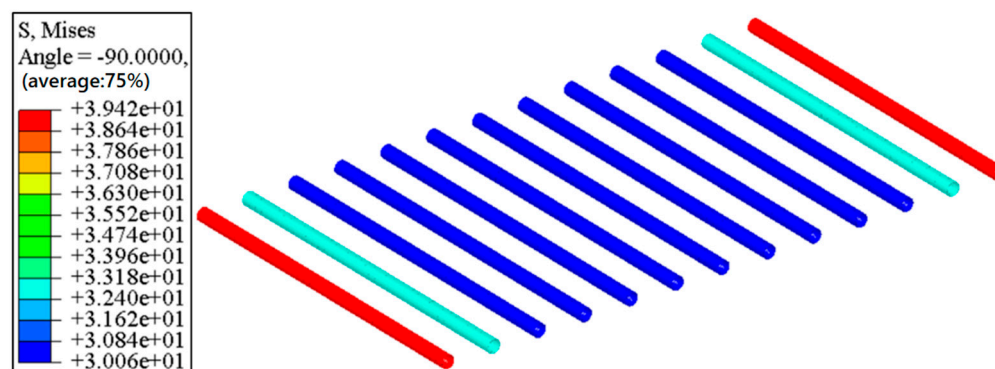


Figure 22. Stress cloud diagram of the second steel bracing in step 6.

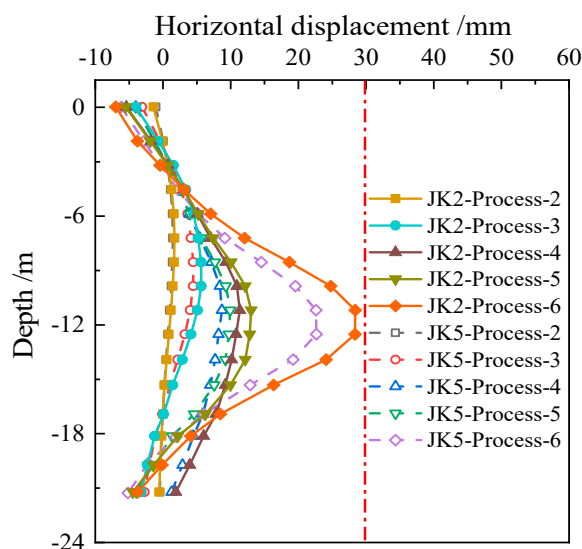


Figure 23. Effect of initial compression stiffness on horizontal displacement of envelope structure.

3.3.3. Influence of Initial Compression Stiffness

As shown in Figure 23, the weakened initial compression stiffness at the DC joint has a greater effect on the horizontal displacement of the enclosure structure, and increasing the initial compression stiffness at the DC joint can significantly improve the control effect of the steel support on the horizontal displacement of the enclosure structure. From the first layer of soil excavation, due to the difference in the initial compression stiffness, the horizontal displacement of the enclosure structure began to produce a difference, and with the application of the pit, the effect of the weakening of the initial compression stiffness on the horizontal deformation of the enclosure structure gradually increased. As shown in Figure 24, the maximum horizontal displacement difference of the enclosure structure between model JK2 and JK5 after the excavation of the first layer of soil is 1.2 mm, while the difference is 5.7 mm after the removal of the third steel support. The weakening of the initial compressive stiffness of the steel support has a significant effect on the horizontal displacement of the enclosure structure.

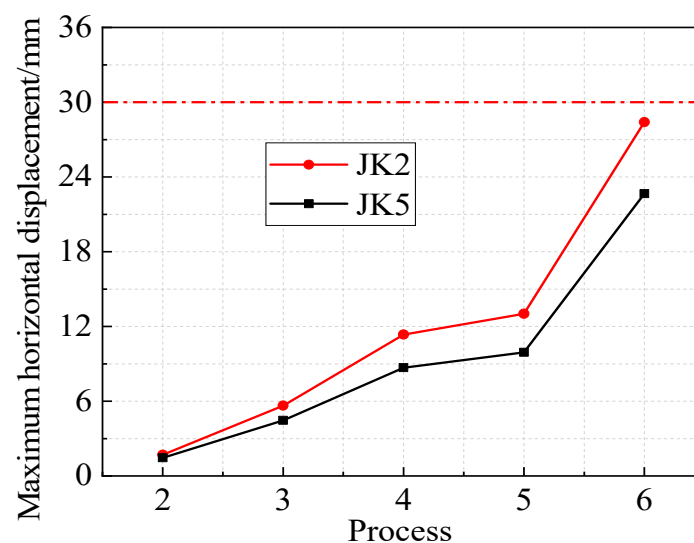


Figure 24. Variation law of maximum horizontal displacement of envelope structure under different initial compression stiffness.

4. Conclusions

This paper describes a quantitative study on the weakening of steel support bearing capacity by DC joints. Through the monitoring data, the pre-axial force holding performance of steel support, the axial force of steel support, the horizontal displacement of the diaphragm wall, and the change rule of the surface settlement around the pit were analyzed in the construction process of a pit of Beijing Metro Line 17; a finite element model corresponding to the pit project was established, and the numerical results were analyzed in comparison with the measured data to validate the reasonableness of the parameter settings in the finite element model. The influence of different local weakening types of steel support on the stability of the enclosure structure was investigated through numerical analysis. The main conclusions are as follows:

1. According to the measured data of the pit using the DC joint, the loss of pre-axial force at the DC joint is serious and mainly occurs at the moment of jack unloading, at which time the loss of pre-axial force is between 20% and 30%. After that, the pre-axial force will be further lost, and the pre-axial force of the steel support is only 67% of the design value when the soil underneath is not excavated within 24 h.
2. On-site monitoring data show that the DC joint is unfavorable for the horizontal displacement control of the pit enclosure structure, and the maximum displacement is more than 31 mm, which exceeds the control standard. At the same time, the

DC joint is unfavorable for the control of surface settlement around the pit, and the accumulated settlement value of the nearest measurement point reaches 53.13 mm, which is close to twice that of the control standard.

3. The DC joint has an obvious weakening effect on steel support. The bearing capacity of the DC joint is much smaller than that of its equivalent steel pipe section. The yield and ultimate loads of the DC joint are about 20% to 70% of that of its equivalent steel pipe section, and the initial compressive stiffness is only about 10% to 20% of that of its equivalent steel pipe section.
4. The pre-axial force and initial bending stiffness of steel support have a greater influence on the stability of the enclosure structure, and the influence of the two on the stability of the enclosure structure becomes more obvious as the process proceeds. When the yield load of steel support is not lower than that of row piles, changing the yield load of the support has no effect on the stability of the enclosure structure.
5. When the soil below the steel support is not excavated for a long time, the loss of pre-axial force is serious, so when the steel support is excavated for a longer period of time after erection, the pre-axial force of all the steel supports should be checked in advance before excavation, and the pre-axial force should be reapplied when the pre-axial force of the steel support is small or the support is not under force.

Author Contributions: Methodology, Z.X.; Software, Z.X., X.N. and J.L.; Validation, J.J.; Investigation, X.L. and C.X.; Resources, X.L.; Data curation, Z.X.; Writing—original draft, Z.X.; Writing—review & editing, X.N. All authors have read and agreed to the published version of the manuscript.

Funding: This research was funded by National Natural Science Foundation of China (grant number 51538001).

Data Availability Statement: Data are contained within the article.

Conflicts of Interest: The authors declare no conflict of interest.

References

1. Luo, Z.; Li, Y.; Zhou, S.; Di, H. Effects of vertical spatial variability on supported excavations in sands considering multiple geotechnical and structural failure modes. *Comput. Geotech.* **2018**, *95*, 16–29. [\[CrossRef\]](#)
2. Cui, X.; Ye, M.; Zhuang, Y. Performance of a foundation pit supported by bored piles and steel struts: A case study. *Soils Found.* **2018**, *58*, 1016–1027. [\[CrossRef\]](#)
3. Li, Z.; Han, M.; Liu, L.; Li, Y.; Yan, S. Corner and partition wall effects on the settlement of a historical building near a supported subway excavation in soft soil. *Comput. Geotech.* **2020**, *128*, 103805. [\[CrossRef\]](#)
4. Lan, W.W.; Li, B.; Zhang, Z.W. Seismic performance of steel-concrete composite structural walls with prestressed internal bracing. *J. Constr. Steel Res.* **2018**, *140*, 11–24. [\[CrossRef\]](#)
5. Goh, A.T.C.; Zhang, R.H.; Wang, W.; Wang, L.; Zhang, W.G. Numerical study of the effects of groundwater drawdown on ground settlement for excavation in residual soils. *Acta Geotech.* **2019**, *15*, 1259–1272. [\[CrossRef\]](#)
6. Quagliaroli, M.; Malerbam, P.G.; Albertin, A.; Pollini, N. The role of prestress and its optimization in cable domes design. *Comput. Struct.* **2015**, *161*, 17–30. [\[CrossRef\]](#)
7. Zhang, M.J.; Yang, M.; Li, P.; Gao, Y.H. Mechanical behaviours of a symmetrical bolt fasten wedge active joint for braced ex-cavations. *Symmetry* **2020**, *12*, 140. [\[CrossRef\]](#)
8. Zhang, M.J.; Xie, Z.T.; Li, P.F. Bearing capacity and failure behavior of disconnectable coupling joint with double row wedges (DCJD) used in the prestressed internal bracing. *Undergr. Space* **2022**, *7*, 498–513. [\[CrossRef\]](#)
9. Ding, Z.; Wang, D.; Yu, X.F.; Wang, J.Y.; Jiang, J.Q. Monitoring and analysis of deep foundation pit at Xintang Road-Jingfang Road cross of Hangzhou metro. *Geotech. Eng.* **2013**, *35*, 445–451. (In Chinese)
10. Sun, J.C.; Bai, T.H. Research on the bearing capacity of the flexible head of the steel support system of the subway foundation excavation. *Constr. Technol.* **2020**, *49*, 119–125. (In Chinese)
11. Xie, Z.T.; Niu, X.K.; Li, P.F.; Zhang, M.J.; Liu, X. Mechanical Properties of Disconnectable Coupling Joints for Steel Bracing under Eccentric Load. *Appl. Sci.* **2023**, *13*, 5596. [\[CrossRef\]](#)
12. Purwanto, E.; Kristiawan, S.A.; Sangadji, S.; Saifullah, H.A. Influence of Joint Strengthening on the Seismic Performance of Non-Engineered Buildings. *Buildings* **2024**, *14*, 488. [\[CrossRef\]](#)
13. Cheng, X.; Zheng, G.; Diao, Y.; Huang, T.; Deng, C.; Nie, D.; Lei, Y. Experimental study of the progressive collapse mechanism of excavations retained by cantilever piles. *Can. Geotech.* **2017**, *54*, 574–587. [\[CrossRef\]](#)
14. Puzrin, A.M.; Alonso, E.E.; Pinyol, N.M. Braced Excavation Collapse: Nicoll Highway, Singapore. In *Geomechanics of Failures*; Springer: Amsterdam, The Netherlands, 2010.

15. Endicott, J. Lessons learned from the collapse of the Nicoll Highway in Singapore April 2004. *IABSE Symp. Rep.* **2013**, *101*, 1–6.
16. Zhang, K.C.; Li, J.M. Accident analysis for “08.11.15” foundation pit collapse of Xianghu Station of Hangzhou metro. *Chin. J. Geotech. Eng.* **2010**, *32* (Suppl. S1), 338–342. (In Chinese)
17. Zhou, Z.; Irizarry, J. Integrated framework of modified accident energy release model and network theory to explore the full complexity of the Hangzhou subway construction collapse. *Manag. Eng.* **2016**, *32*, 5016013. [[CrossRef](#)]
18. Li, G.X. Discussion on Accident of Foundation Excavation of Xianghu Station of Hangzhou Subway No. 1 Line Again. *Geotech. Eng. Tech.* **2015**, *29*, 273–279. (In Chinese)
19. Zhang, M.J.; Jian, J.L.; Li, P.F.; Wu, H.; Li, J.S. Field Test on the BFW Active Joint of Steel Support in Foundation Pit Engineering. *Chin. J. Undergr. Space Eng.* **2022**, *18*, 538–545. (In Chinese)
20. Xie, Z.T. *Study on Bearing Capacity and Improvement Measures of Steel Bracing System in Subway Foundation Pit Engineering*; Beijing University of Technology: Beijing, China, 2021. (In Chinese)
21. Zhang, M.J.; Xie, Z.T.; Li, P.F. Experimental and numerical investigation on the bearing capacity of disconnectable coupling (DC) joints for prestressed internal bracing in subway excavations. *Tunn. Undergr. Space Technol.* **2020**, *104*, 103501. [[CrossRef](#)]
22. Tian, F.; Liu, C.; Liu, F.; Luo, W.; Deng, R.; Chen, S.; Luo, Y. Research on the True stress-strain Curve of Q235 Steel. *J. Cent. South Univ. For. Technol.* **2011**, *31*, 182–186.
23. Yang, Y. *Study on Hysteresis Performance of ALC Wallboard Embedded in Steel Structure Residence*; Huazhong University of Science and Technology: Wuhan, China, 2023. (In Chinese)

Disclaimer/Publisher’s Note: The statements, opinions and data contained in all publications are solely those of the individual author(s) and contributor(s) and not of MDPI and/or the editor(s). MDPI and/or the editor(s) disclaim responsibility for any injury to people or property resulting from any ideas, methods, instructions or products referred to in the content.